Polymer Chemistry

COMMUNICATION

View Article Online
View Journal | View Issue

Cite this: *Polym. Chem.*, 2020, **11**, 292

Received 16th August 2019,
Accepted 4th October 2019

DOI: 10.1039/c9py01235d

rsc.li/polymers

Forcing single-chain nanoparticle collapse through hydrophobic solvent interactions in comb copolymers†

Cheyenne H. Liu, ‡ Logan D. Dugas,‡ Jared I. Bowman, Tamuka Chidanguro, Robson F. Storey and Yoan C. Simon *

We introduce a novel synthetic strategy in which high molecular weight comb copolymers with aliphatic side chains can collapse into single-chain nanoparticles (SNCPs) *via* photodimerization of anthracene under ultraviolet (UV) irradiation. By deliberately selecting hydrophobic comonomers with disparate solvency, we demonstrated that we could control chain collapse. We attribute these results to the formation of pseudo-unimicellar structures, whereby polyisobutylene (PIB) side chains are preferentially solvated, thereby compressing anthracene moieties to form a denser crosslinked core. The control of hydrophobic interactions is a common occurrence in proteins and we believe that our approach can be further extended to achieve multi-compartment SCNPs whereby each section is responsible for a given function.

Nature is precise and elegant in stringing together amino acids into primary structures with well-defined hydrophilic and hydrophobic segments. This compositional precision in proteins allows for direct and assisted folding of the primary structures into more complex secondary, tertiary, and quaternary structures for a variety of necessary biological functions, including enzymatic activity, DNA replication, and cascade signaling.[1–3] Systematic control of polymeric sequencing is an ongoing challenge that has undergone several advances in recent years;[4–6] however, most synthetic polymer strategies lack the sophistication achieved in nature and often rely on cruder approaches to achieve functionality in artificial systems.[4,7–11] In recent years, methodologies involving single-chain nanoparticles (SCNPs) have emerged to emulate protein functionality.[5,7,12–16] SCNPs are single polymer chains, collapsed *via* intrachain crosslinks, which resemble proteins in many ways: their collapse is kindred to protein folding; their crosslinks are reminiscent of disulfide bridges, and the introduction of catalytic sites is comparable to active enzymatic pockets.[6,17,18] Consequently, the scientific pursuit of SCNPs has grown unabated in areas such as catalysis,[17,19–21] sensing,[22–24] and site-specific drug delivery.[25–27]

To realize the full potential of SCNPs, one must understand the parameters governing chain collapse. Seminal work by Pomposo and coworkers laid the theoretical framework for the understanding of how solvent selection affects the ultimate size and structure of SCNPs.[28–31] They meticulously explored through computational modeling whether SCNPs can form true globular structures.[28,29,31–33] Namely, they showed that one can currently describe SCNPs as noncompact objects, whose morphology is dominated by intrachain crosslinking of nearby segments rather than true globular collapse.[19,31] Lo Verso *et al.* further suggested two models by which one could achieve a globular conformation of SCNPs.[31] In the first, chains are anchored to solid supports at low surface coverage to avoid intermolecular bonding, while in the second a solvophobic/solvophilic copolymer helps achieve a core–shell conformation, an approach that piqued our interest and that we exploit herein.[31]

Traditionally, SCNPs stem from linear polymeric chains that lack any secondary structure. Palmans and coworkers have capitalized on the introduction of short hydrophilic oligo (ethylene glycol) or Jeffamine® chains to promote collapse.[17,19,22,34] The aforementioned systems are polymer combs, *i.e.* copolymers with low graft density, bearing short oligomeric side chains. Their work illustrated the effect of solvent selection when considering the collapse of amphiphilic comb copolymers with non-covalent crosslinks.[17,34] Furthermore, Basasoro *et al.* have readily tuned the internal structure and topology of SCNPs *via* transfer from selective to good (nonselective) solvent conditions.[30] They achieved chain collapse by introducing Cu(II) into poly[methoxy(oligo(ethylene glycol) methacrylate-*co*-2-acetoacetoxyethyl methacrylate].[30]

The utilization of disparate solvency is clearly a promising strategy to further drive intrachain crosslinking in comb

School of Polymer Science and Engineering, The University of Southern Mississippi, 118 College Drive #5050, Hattiesburg, MS 39406, USA.
E-mail: yoan.simon@usm.edu

†Electronic supplementary information (ESI) available. See DOI: 10.1039/c9py01235d

‡These authors contributed equally in the completion of this work.

architecture polymers beyond mere dilution.[28–31,33,34] However, most strategies to date have been limited to hydrophobic/hydrophilic interactions. To achieve more complex architectures and better understand the limitations of collapse in SCNPs, there is a need to explore other solvency effects, particularly when one considers that most industrial polymers are hydrophobic in nature. Furthermore, the degree of polymerization of the side chains DP_{sc} has been restricted to short oligomers (<1100 g mol^{-1}).[17,34,35] The natural assumption is that short oligomeric chains would inherently be less sterically restrictive, allowing for greater degrees of crosslinking. Solvent choice can however greatly affect the compartmentalization of crosslinking moieties.[29,30] It may be thus advantageous to expand the DP_{sc} to better take advantage of solvophilic and solvophobic effects. Finally, we have used photochemical crosslinking, a common tool for SCNP fabrication,[36–40] as a means to covalently lock the collapsed state into place.

Taking into consideration these precepts, we synthesized comb copolymers (Fig. 1) by ring-opening metathesis polymerization (ROMP) of oxanorbornene maleimide polyisobutylene (oNBMIPIB) and anthracen-9-ylmethyl bicyclo[2.2.1]hept-5-ene-2-carboxylate (NB-An). Comonomer feed was 20 or 40 mol% anthracene-containing comonomer. We chose PIB as a building block due to its affinity for non-polar aliphatic solvents and ease of end-functionalization. As a result, we were able to create SCNPs *via* photo-dimerization, either by sequential UV-irradiation in tetrahydrofuran (THF) solution followed by *n*-hexane solution (Fig. 1), or directly in a 50/50 (v/v) THF/*n*-hexane mixture. We monitored the extent of the dimerization and the decrease in hydrodynamic volume *via* size-exclusion chromatography (SEC), UV/Vis, and 90° dynamic light scattering (DLS).

Following procedures reported by Storey and coworkers, we synthesized oNBMIPIB (M_n = 3.5 kg mol^{-1}, $Đ$ = 1.21) in three steps: living cationic polymerization of isobutylene using $TiCl_4$ as the Lewis-acid catalyst, *in situ* end-functionalization *via* Friedel–Crafts alkylation of (3-bromopropoxy)benzene, and nucleophilic substitution (S_N2) of bromide with oxanorbornene dicarboximide.[41,42] Gratifyingly, ^{1}H NMR spectra showed the expected quantitative shift of the –CH_2Br protons from 3.55 to 3.63 ppm upon reaction with the imide moiety (Fig. S3 and S4†), indicating complete substitution of the primary bromide terminus. A shift towards shorter elution time by size-exclusion chromatography (Fig. S5†) further corroborated the occurrence of the S_N2 reaction. Matrix-assisted laser desorption ionization time of flight (MALDI-TOF) mass spectrometry also demonstrated complete chain-end substitution (Fig. S6 and S7†) albeit with the apparent loss of furan due to the high vacuum and laser energy output (*ca.* 43 μJ) during MALDI, as previously reported in literature.[41]

We synthesized NB-An by reacting an *endo*/*exo* mixture of norbornene carboxylic acid with 9-anthracene methanol *via* Steglich esterification in dichloromethane (DCM). We observed the simultaneous quantitative disappearance of the hydroxy signal at 1.77 ppm and the shift of the methylene α to the anthracene from 5.47 to 5.82 (*exo*) and 6.16 ppm (*endo*) upon esterification (Fig. S8†). NB-An was then polymerized in DCM using third-generation Grubbs ruthenium alkylidene (G3) as a catalyst. Fig. S10† shows the ^{1}H NMR spectrum of poly(NB-An) (PNB-An) obtained in this manner. Despite the presence of mixed *endo*/*exo* diastereomers, the SEC elugram showed that the polymerization proceeded as expected ($M_{n,target}$ = 65.6 kg mol^{-1} and $M_{n,exp}$ = 70.2 kg mol^{-1}, $Đ$ = 1.06), albeit with a minute high-molecular-weight shoulder (Fig. S11†).

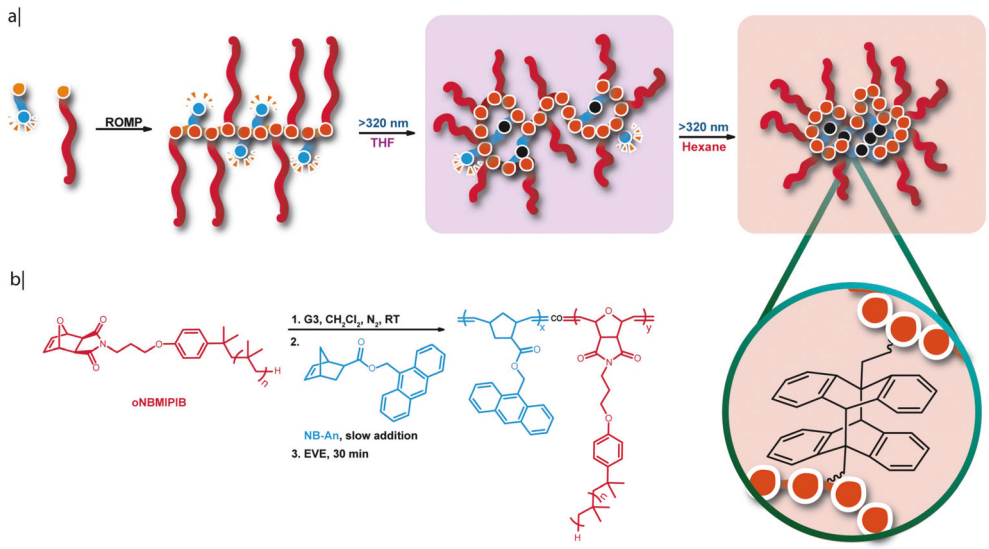

Fig. 1 a| Illustration of the polymerization and subsequent light-induced intrachain crosslinking of anthracene-substituted comb copolymers. Further photodimerization is favored by solvency. The purple box represents a good solvent for both comonomers (*i.e.* THF) while the orange box represents a good solvent for the polyisobutylene grafts only (*i.e.* hexane). b| Synthetic scheme showing the ring-opening metathesis copolymerization (ROMP) of oNBMIPIB and NB-An to generate photodimerizable comb copolymers.

To inform copolymerization strategy, we investigated reactivity of the NB-An comonomer compared to that of oNBMIPIB. We monitored polymerization kinetics of the former in *d*2-DCM using *in situ* ^{1}H NMR spectroscopy, by relative integration of the proton signal of anthracene at the 10-position at 8.57 ppm (1H) compared to the total combined aromatic proton peaks of NB-An and the copolymer between 7.14 to 8.57 ppm (9H + 9H) (Fig. S12†). Fig. S13† shows a plot of conversion *vs.* time, representing the average of three individual polymerizations. We obtained the value of the apparent first-order rate constant, $k_{obs} = 5.81 \times 10^{-3}$ s^{-1}, from the slope of a plot of $\ln([M]_0/[M])$ *vs.* *t*, where $[M]_0$ is the initial monomer concentration and [M] is the monomer concentration at time *t* (Fig. S14 and Table S1†). Yang *et al.* previously reported a rate constant of $k_{obs} = 2.33 \times 10^{-3}$ s^{-1} for ROMP of oNBMIPIB, and we have used this value as a reasonable estimate for the rate constant of our oNBMIPIB.[41] Although the molecular weight of the latter is somewhat lower than that of Yang *et al.* (M_n = 3.5 *vs.* 4.2 kg mol^{-1}), we assumed similar rate constants of polymerization on account of the work of Radzinski *et al.*, who showed that the rate in G3-initiated ROMP of macromonomers is dependent on the *anchor group* selected but less sensitive to small differences in side-chain molecular weight.[43]

To offset the rate differences and ensure good distribution of anthracene moieties along the backbone, we synthesized PNB-An-*co*-PoNBMIPIB comb copolymers by slow addition of NB-An into a vial containing oNBMIPIB and G3 in DCM (Table 1). Specifically, we targeted two compositions, 20 (P1) and 40 (P2) mol% of anthracene in the copolymers, and a constant degree of polymerization of the backbone, DP_{bb} = 150 was targeted. We confirmed the successful copolymerization of oNBMIPIB and NB-An by observing the characteristic shifts of the monomeric alkene in the ^{1}H NMR spectrum from 6.49 to 6.07 ppm for oNBMIPIB and the shift of the proton signal of anthracene at the 10-position from 8.50 to 8.27 ppm for NB-An (Fig. S15 and S16†). The polymers were found to be of high molecular weight *via* SEC (Fig. S17†) with 12 and 32% molar incorporation of NB-An *via* ^{1}H NMR. We note that, in retrospect, our rate of addition of NB-An was probably too low, leading not to statistical but rather to gradient copolymers initially rich in oNBMIPIB. Nevertheless, the NB-An moieties proved to be sufficiently dispersed over the entire copolymer to achieve the unique conformational effects described herein.

We began the process of intrachain dimerization by irradiating our comb copolymers in a favorable solvent for both comonomers, *i.e.* THF, under dilute conditions (c = 1 mg mL^{-1}) using a UV light source (λ = 366 nm, 8 W). We measured UV-vis absorbance spectra at five-minute intervals during irradiation (Fig. 2a) and monitored the decrease of the anthracene peak ($\lambda_{max} \approx 365$ nm) upon photodimerization until the change in absorbance between consecutive intervals was less than 0.005 a.u. For P1, the decrease in the absorption band at $\lambda_{max} \approx 365$ nm corresponds to a 64% conversion of the anthracene to its photodimer. SEC elugrams displayed a shift to longer retention time upon irradiation for both the in-line refractive index (RI, Fig. 2b) and multi-angle laser light scattering (MALLS, Fig. S21†) detectors. In dynamic light scattering, the hydrodynamic radius (R_h) of P1 decreased from 12.95 ± 1.75 nm to 10.14 ± 0.95 nm, a moderate yet statistically significant change (Fig. 2c). Based on literature precedent,[26,28,30] we hypothesized that the addition of an unfavorable solvent for anthracene would further drive the collapse of the chain, simultaneously decreasing the R_h and enabling further dimerization. We found experimentally that NB-An was insoluble in *n*-hexane. Conversely, *n*-hexane is an excellent solvent for the large PIB side chains. Accordingly, the PIB side chains should be preferentially solvated while the anthracene segments should be contracted. Consequently, we added 1 mL of *n*-hexane to 1 mL of the previously irradiated solution in THF to form a *ca.* 50/50 (v/v) THF/*n*-hexane solution (c = 0.5 mg mL^{-1}). After five minutes of equilibration, we subjected the P1 solution to a second irradiation until the change in absorbance between consecutive intervals was less than 0.005 a.u. Since the absorbance spectrum of the irradiated solution of P1 would automatically decrease upon dilution with *n*-hexane, for reference purposes, we incorporated the spectrum of a solution of pristine P1 (c = 1 mg mL^{-1}) in THF diluted 50/50 (v/v) with *n*-hexane (Fig. 2d, blue: c = 0.5 mg mL^{-1}). As predicted, the cosolvent system enabled us to drive the reaction forward with the absorbance decreasing additionally by *ca.* 31%, pushing the total conversion of anthracene dimerization to *ca.* 75% over the two irradiations (Fig. 2d). Note that baseline adjustment was necessary to correct the minor inconsistencies in UV-vis spectroscopy in the cosolvent systems (Fig. S18–20†). The increase in crosslinks was further corroborated by DLS, which showed a further compaction in R_h down to 9.88 ± 0.80 nm, as compared to the original R_h value of 12.95 ±

Table 1 Theoretical and experimental compositions and molecular weights of synthesized (co)polymers

	Theoretical					Experimental					
Polymer	Mol% NB-An	$DP_{n,th}$	$DP_{n,th,NBAn}$	$DP_{n,th,oNBMIPIB}$	M_n [a]	Mol% NB-An[b]	$DP_{n,NBAn}$	$DP_{n,oNBMIPIB}$	M_n [a,c]	M_w [a,c]	$Đ$
P1	20	150	30	120	423	12.3	18	132	463	549	1.18
P2	40	150	60	90	330	32.0	48	102	326	405	1.24
PNB-An	100	200	200	—	65	100	213	—	70.2	74.9	1.06

[a] kg mol^{-1}. [b] Determined from ^{1}H NMR (600 MHz, 25 °C). [c] Corresponding d*n*/d*c* values were obtained assuming 100% mass recovery from the refractive index detector.

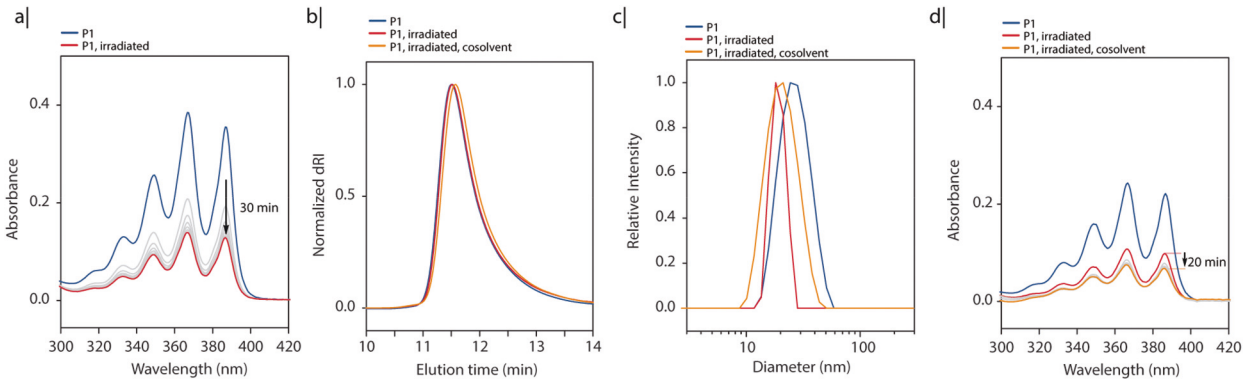

Fig. 2 a| UV-vis spectra showing the evolution of intrachain crosslinking during photodimerization of P1 in THF (c = 1 mg mL^{-1}). The time on the black arrow indicates the duration of irradiation. b| Size-exclusion chromatogram of the differential refractive index (dRI) responses showing the shift towards longer elution time. c| Normalized distribution of sizes by DLS of pristine P1 (blue), irradiated P1 in THF (c = 1 mg mL^{-1}, red), and irradiated P1 in 50/50 (v/v) THF/hexane (c = 0.5 mg mL^{-1}, orange). d| UV-vis spectra showing the evolution of the photodimerization of anthracene in P1 in 50/50 (v/v) THF/hexane (c = 0.5 mg mL^{-1}). The time on the black arrow indicates the duration of irradiation. Note that the blue spectrum in d| is a solution of pristine P1 in 50/50 (v/v) THF/hexane.

1.75 nm and 10.14 ± 0.95 after the first irradiation. Likewise, the SEC trace of P1 showed a marked shift to a longer elution time after the second irradiation (Fig. 2b). Interestingly, the second UV treatment seemingly led to a broadening of the distribution in DLS; whereas SEC elugrams appeared to only show shifts towards longer elution times even with the MALLS detector (Fig. S21†). We therefore attribute this discrepancy to the excessive sensitivity of DLS to larger particles.

During the first irradiation of copolymer P2 in THF, the dimerization reached *ca.* 80% conversion by UV-vis; the SEC elugram shifted towards longer retention time (in both RI and MALLS detection), and the R_h contracted to 9.66 ± 0.65 nm, from 11.02 ± 1.06 nm (Fig. 3a–c and Fig. S22†). We surmised that the higher content of anthracene would eventually lead to more compaction upon addition of *n*-hexane due to solvophobic interactions and enhanced segmental flexibility. Gratifyingly, the addition of the unfavorable *n*-hexane had a significant effect in reducing the R_h down to 8.32 ± 0.57 nm (Fig. 3c) and further pushing the total photocycloaddition conversion by another 28% to *ca.* 86% over the two irradiations (Fig. 3d). This transformation illustrates that through deliberate solvent selection, the intrachain crosslinking of comb copolymers may be modularly driven to lower hydrodynamic volumes and ultimately generate solvent-selective single chain nanoparticles.

To understand the role of solvency on comb copolymer collapse, we repeated the UV irradiation experiments of P1 in pure *n*-hexane, where aggregation was expected to occur due to the insolubility of NB-An repeat units in *n*-hexane. A solution of P1 in *n*-hexane (c = 1 mg mL^{-1}) underwent the same irradiation procedure for 30 min and reached a dimerization

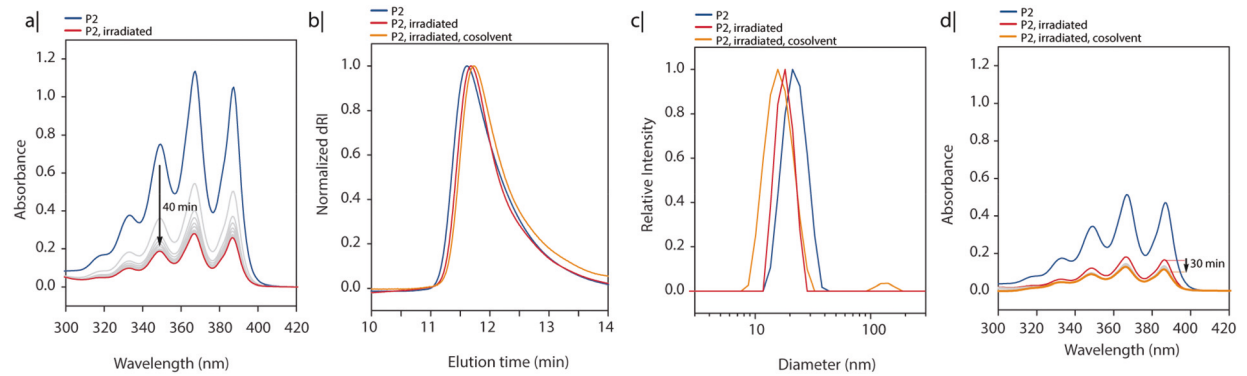

Fig. 3 a| UV-vis spectra showing the evolution of the photodimerization of anthracene in P2 in THF (c = 1 mg mL^{-1}). The time on the black arrow indicates the duration of irradiation. b| Size-exclusion chromatogram of the differential refractive index (dRI) response showing the shift towards longer elution time and c| normalized distribution of sizes by DLS, respectively, of pristine P2 (blue), irradiated P2 in THF (c = 1 mg mL^{-1}, red), and irradiated P2 in 50/50 (v/v) THF/hexane (c = 0.5 mg mL^{-1}, orange) and d| UV-vis spectra showing the evolution of the photodimerization of anthracene in P2 in 50/50 (v/v) THF/hexane (c = 0.5 mg mL^{-1}). The time on the black arrow indicates the duration of irradiation. Note that the blue spectrum in d| is a solution of pristine P2 in 50/50 (v/v) THF/hexane.

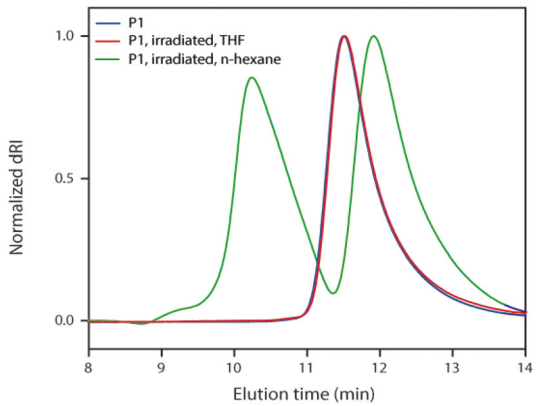

Fig. 4 Size-exclusion chromatogram of the differential refractive index (dRI) response of pristine P1 (blue), P1 irradiated in THF (c = 1 mg mL^{-1}, red), and P1 irradiated in pure n-hexane (c = 1 mg mL^{-1}, green).

conversion of only *ca.* 46% (Fig. S35†). We could identify a large peak at approximately 10 min in SEC (Fig. 4 and S37†), and a correspondingly large R_h *via* DLS (77.4 ± 2.3 nm) (Fig. S38†). Concomitantly, we observed a second elution peak at 12 min in SEC (Fig. 4), which represents a lower hydrodynamic volume when compared to the pristine and twice-irradiated sample. However, we could not observe this marked compaction in DLS (R_h = 12.1 ± 0.69 nm) (Fig. S38†). We made similar observations for P2 (Fig. S41–44†). Together these results indicate that, although a significant fraction of aggregation occurs in n-hexane, disparate solvency in crosslinkable comb copolymers is an inspired choice to tune chain collapse and obtain multiple compartments from a single comb copolymer. We are currently investigating further the influence of solvent quality on the nature of the SCNPs.

In summary, we have demonstrated to the best of our knowledge the first collapse of purely hydrophobic comb copolymers with large oligomeric aliphatic side chains through the photo-dimerization of pendant anthracene units. By increasing the ratio of nonsolvent for the small-molecule crosslinking comonomer, we achieved greater degrees of intrachain crosslinking, which reduced the R_h of our SCNPs substantially. This work leads us to believe that through clever selection of the side chains and orthogonal chemistry, we may achieve SCNPs that are multi-compartment in which each individual compartment contains a unique chemical function.

Conflicts of interest

The authors declare no conflicts of interest.

Acknowledgements

C. H. L. acknowledges support from the National Science Foundation Research Trainee (NSF NRT) Program Award #1449999. The authors acknowledge support from the American Chemical Society Petroleum Research Fund (ACS PRF) grant #57957. This material is based on work in part supported by the National Science Foundation under Grant No. (1757220). The authors would like to acknowledge the help of Eric R. King and Dr. Dwaine Braasch for their assistance in running the UV-vis instrumentation.

Notes and references

1 Y. Ravikumar, S. P. Nadarajan, T. H. Yoo, C. S. Lee and H. Yun, *Trends Biotechnol.*, 2015, **33**, 462–470.
2 A. Aze and D. Maiorano, *F1000Research*, 2018, **7**, 1351.
3 M. Katoh, *Oncol. Rep.*, 2005, **14**, 1583–1588.
4 M. Ouchi, N. Badi, J. F. Lutz and M. Sawamoto, *Nat. Chem.*, 2011, **3**, 917–924.
5 M. Zamfir and J. F. Lutz, *Nat. Commun.*, 2012, **3**, 1–8.
6 J. Niu, R. Hili and D. R. Liu, *Nat. Chem.*, 2013, **5**, 282–292.
7 J. P. Cole, J. J. Lessard, K. J. Rodriguez, A. M. Hanlon, E. K. Reville, J. P. Mancinelli and E. B. Berda, *Polym. Chem.*, 2017, **8**, 5829–5835.
8 G. Gody, T. Maschmeyer, P. B. Zetterlund and S. Perrier, *Nat. Commun.*, 2013, **4**, 1–9.
9 S. Hecht, *Mater. Today*, 2005, **8**, 48–55.
10 B. Lewandowski, G. De Bo, J. W. Ward, M. Papmeyer, S. Kuschel, M. J. Aldegunde, P. M. E. Gramlich, D. Heckmann, S. M. Goldup, D. M. D'Souza, A. E. Fernandes and D. a. Leigh, *Science*, 2013, **339**, 189–193.
11 R. E. Connor and D. A. Tirrell, *Polym. Rev.*, 2007, **47**, 9–28.
12 C. K. Lyon, A. Prasher, A. M. Hanlon, B. T. Tuten, C. A. Tooley, P. G. Frank and E. B. Berda, *Polym. Chem.*, 2015, **6**, 181–197.
13 O. Altintas and C. Barner-Kowollik, *Macromol. Rapid Commun.*, 2016, **37**, 29–46.
14 J. He, L. Tremblay, S. Lacelle and Y. Zhao, *Soft Matter*, 2011, **7**, 2380–2386.
15 H. Frisch, J. P. Menzel, F. R. Bloesser, D. E. Marschner, K. Mundsinger and C. Barner-Kowollik, *J. Am. Chem. Soc.*, 2018, **140**, 9551–9557.
16 A. M. Hanlon, C. K. Lyon and E. B. Berda, *Macromolecules*, 2016, **49**, 2–14.
17 E. Huerta, P. J. M. Stals, E. W. Meijer and A. R. A. Palmans, *Angew. Chem., Int. Ed.*, 2013, **52**, 2906–2910.
18 A. Sanchez-Sanchez, A. Arbe, J. Colmenero and J. A. Pomposo, *ACS Macro Lett.*, 2014, **3**, 439–443.
19 M. Artar, T. Terashima, M. Sawamoto, E. W. Meijer and A. R. A. Palmans, *J. Polym. Sci., Part A: Polym. Chem.*, 2014, **52**, 12–20.
20 B. van Genabeek, P. J. M. Stals, E. Huerta, A. R. A. Palmans and E. W. Meijer, *Macromol. Rapid Commun.*, 2014, **35**, 1320–1325.
21 J. Chen, J. Wang, K. Li, Y. Wang, M. Gruebele, A. L. Ferguson and S. C. Zimmerman, *J. Am. Chem. Soc.*, 2019, **141**, 9693–9700.

22 M. A. J. Gillissen, I. K. Voets, E. W. Meijer and A. R. A. Palmans, *Polym. Chem.*, 2012, **3**, 3166–3174.
23 K. Rurack, *Spectrochim. Acta, Part A*, 2001, **57**, 2161–2195.
24 G. K. Walkup and B. Imperiali, *J. Am. Chem. Soc.*, 1997, **119**, 3443–3450.
25 R. J. Passarella, D. E. Spratt, A. E. Van Der Ende, J. G. Phillips, H. Wu, V. Sathiyakumar, L. Zhou, D. E. Hallahan, E. Harth and R. Diaz, *Cancer Res.*, 2010, **70**, 4550–4559.
26 A. Sanchez-Sanchez, A. Arbe, A. J. Moreno, J. Colmenero, J. A. Pomposo, S. Akbari, A. Etxeberria and U. Gasser, *ACS Macro Lett.*, 2013, **2**, 491–495.
27 A. P. P. Pia, P. Kröger, N. M. Hamelmann, A. Juan, S. Lindhoud and J. M. J. Paulusse, *ACS Appl. Mater. Interfaces*, 2018, **10**, 30946–30951.
28 J. A. Pomposo, I. Perez-Baena, F. Lo Verso, A. J. Moreno, A. Arbe and J. Colmenero, *ACS Macro Lett.*, 2014, **3**, 767–772.
29 J. A. Pomposo, A. J. Moreno, A. Arbe and J. Colmenero, *ACS Omega*, 2018, **3**, 8648–8654.
30 S. Basasoro, M. Gonzalez-burgos, A. J. Moreno, F. Lo Verso, A. Arbe, J. Colmenero and J. A. Pomposo, *Macromol. Rapid Commun.*, 2016, **37**, 1060–1065.
31 F. Lo Verso, J. A. Pomposo, J. Colmenero and A. J. Moreno, *Soft Matter*, 2015, **11**, 1369–1375.
32 J. W. Liu, M. E. MacKay and P. M. Duxbury, *EPL*, 2008, **84**, 46001.
33 E. Guazzelli, E. Martinelli, G. Galli, L. Cupellini, S. Jurinovich and B. Mennucci, *Polymer*, 2019, **161**, 33–40.
34 G. M. Ter Huurne, M. A. J. Gillissen, A. R. A. Palmans, I. K. Voets and E. W. Meijer, *Macromolecules*, 2015, **48**, 3949–3956.
35 Y. Zhu, R. Batchelor, A. B. Lowe and P. J. Roth, *Macromolecules*, 2016, **49**, 672–680.
36 P. G. Frank, B. T. Tuten, A. Prasher, D. Chao and E. B. Berda, *Macromol. Rapid Commun.*, 2014, **35**, 249–253.
37 G. W. Breton and X. Vang, *J. Chem. Educ.*, 1998, **75**, 81–82.
38 T. Chidanguro, D. R. Blank, A. Garrett, C. M. Reese, J. M. Schekman, X. Yu, D. L. Patton, N. Ayres and Y. C. Simon, *Dalton Trans.*, 2018, **47**, 8663–8669.
39 S. Telitel, E. Blasco, L. D. Bangert, F. H. Schacher, A. S. Goldmann and C. Barner-Kowollik, *Polym. Chem.*, 2017, **8**, 4038–4042.
40 Y. Fei, C. Liu, G. Chen and C. Hong, *Polym. Chem.*, 2019, **10**, 3895–3901.
41 B. Yang, B. A. Abel, C. L. McCormick and R. F. Storey, *Macromolecules*, 2017, **50**, 7458–7467.
42 D. L. Morgan, N. Martinez-Castro and R. F. Storey, *Macromolecules*, 2010, **43**, 8724–8740.
43 S. C. Radzinski, J. C. Foster, R. C. Chapleski, D. Troya and J. B. Matson, *J. Am. Chem. Soc.*, 2016, **138**, 6998–7004.